ACSNANO
www.acsnano.org
ARTICLE

Efficient CO Oxidation Using Dendrimer-Encapsulated Pt Nanoparticles Activated with <2% Cu Surface Atoms

Long Luo,[†] Liang Zhang,[†,‡] Zhiyao Duan,[†,‡] Aliya S. Lapp,[†] Graeme Henkelman,*[,†,‡] and Richard M. Crooks*[,†,§]

[†]Department of Chemistry, [‡]Institute for Computational and Engineering Sciences, and [§]Texas Materials Institute, The University of Texas at Austin, 105 East 24th Street, Stop A5300, Austin, Texas 78712-1224, United States

Supporting Information

ABSTRACT: In this paper, we show that the onset potential for CO oxidation electrocatalyzed by ~2 nm dendrimer-encapsulated Pt nanoparticles (Pt DENs) is shifted negative by ~300 mV in the presence of a small percentage (<2%) of Cu surface atoms. Theory and experiments suggest that the catalytic enhancement arises from a cocatalytic Langmuir−Hinshelwood mechanism in which the small number of Cu atoms selectively adsorb OH, thereby facilitating reaction with CO adsorbed to the dominant Pt surface. Theory suggests that these Cu atoms are present primarily on the (100) facets of the Pt DENs.

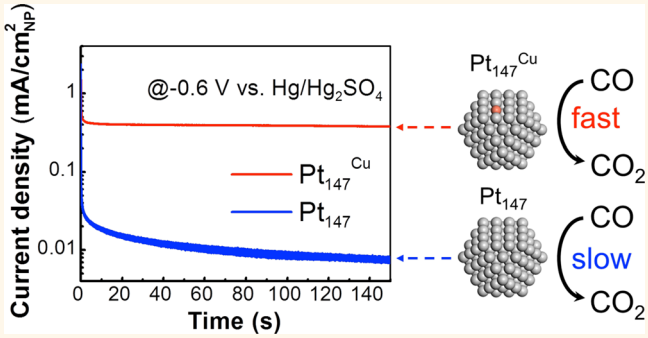

KEYWORDS: *bimetallic nanoparticle, CO electro-oxidation, density functional theory, isolated Cu*

A significant impediment to the development of Pt-based fuel cells is CO poisoning of the Pt electrocatalyst.[1−30] This is a problem in H_2 fuel cells because H_2 is usually obtained by natural gas reforming and CO is a byproduct of that process. CO is also present in fuel cells that burn methanol, formic acid, and other carbon fuels because it is formed as an intermediate during fuel oxidation. The most viable approach for reducing the impact of CO poisoning is to further oxidize it to CO_2, which is much less strongly adsorbed to Pt.

Oxidation of CO occurs through a Langmuir−Hinshelwood (L−H) mechanism (Scheme 1, where M = M′ = Pt), in which adsorbed CO (CO_{ads}) reacts with adsorbed oxygenated species (usually OH) to form CO_2.[1,17,28] However, strong binding of CO to Pt results in a low surface coverage of OH, slow conversion of CO to CO_2, and consequently fewer active sites available for catalyzing the main fuel cell reaction(s). In contrast, Pt alloys with certain other metals (Scheme 1, where M = Pt and M′ = Ru,[1−5,9,25,31,32] Os,[26] Cu,[30,33] Sn, or Bi[6,10,16]) have been found to significantly improve CO tolerance. Such binary catalysts are thought to decrease the number of catalyst sites blocked by CO_{ads} by increasing the surface concentration of OH on the non-Pt metal (M′) and hence the rate of CO oxidation. Accordingly, there are a higher number of Pt sites available at steady state to catalyze the principal fuel cell reaction.

In this paper, we report that the catalytic activity of dendrimer-encapsulated Pt nanoparticles (Pt DENs) toward

Scheme 1

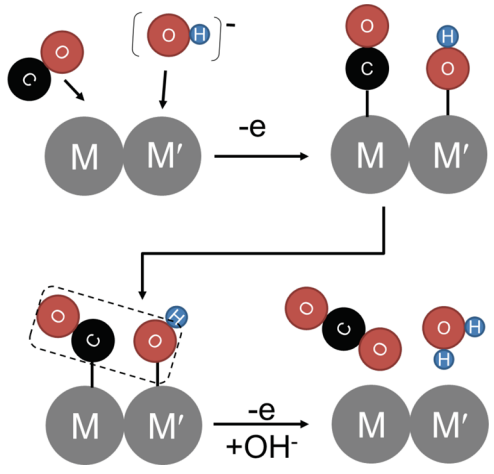

CO electro-oxidation in alkaline solution is dramatically improved after activation by electrochemical Cu underpotential deposition (UPD).[34] Specifically, our experiments show that improved activity after Cu UPD activation originates from a

Received: July 5, 2016
Accepted: August 23, 2016
Published: September 1, 2016

DOI: 10.1021/acsnano.6b04448
ACS Nano 2016, 10, 8760−8769

small number of active sites on the Pt DEN surfaces (<1 site per facet). Density functional theory (DFT) calculations suggest that these special sites comprise individual Cu atoms surrounded by Pt on the (100) facets of the DENs. DFT also indicates that these Cu sites are thermodynamically stable, have ~1 eV lower CO binding energy, and have ~0.2 eV higher affinity for OH binding than the Pt sites. Accordingly, oxidation of CO adsorbed onto Pt atoms is facilitated by the presence of nearby OH groups located on Cu atoms. This finding is significant because it represents an unusual example of trace amounts of a cocatalytic metal producing a dramatic improvement in catalytic performance.[35−37] It also demonstrates how DFT calculations, coupled with experiments, can be used to search for the most likely location of active Cu sites on nanoparticles.

RESULTS AND DISCUSSION

Catalyst Preparation. The DENs in this study were synthesized and characterized using a previously reported method.[38] Briefly, the DENs were prepared by adding 147 equiv of K_2PtCl_4 to a 10 μM solution of a sixth-generation, hydroxyl-terminated poly(amidoamine) dendrimer (G6-OH). After 3 days, this leads to complexation between Pt^{2+} and G6-OH and formation of a precursor denoted as G6-OH-$(Pt^{2+})_{147}$.[38] Reduction of this species using a 10-fold excess of 1.0 M $NaBH_4$ dissolved in 0.3 M NaOH leads to G6-OH(Pt_{147}) DENs. Note that this designation is not intended to suggest that each DEN contains exactly 147 atoms but rather the Pt^{2+}:G6-OH ratio used to prepare them. The G6-OH(Pt_{147})-DENs (hereafter, Pt_{147} DENs) have a measured average size of 1.7 ± 0.4 nm (Figure S1), which is close to the calculated size of cuboctahedral Pt nanoparticles containing 147 Pt atoms (1.6 nm).[38]

Pt_{147} DENs were immobilized onto a glassy carbon rotating disk electrode (GC-RDE) for electrocatalysis measurements. This was done by mixing Pt_{147} DENs with Vulcan EC-72R carbon and then sonicating for 5 min to produce a uniform black ink. Next, 5.0 μL of this ink was drop-cast onto a freshly polished GC-RDE and dried under flowing N_2. Following our previously reported method, we deposited a monolayer of Cu onto just the (100) facets of the Pt_{147} DENs by UPD to yield Pt_{147}@$Cu_{partial}$ DENs (Figure 1, top).[39,40] Specifically, the Pt_{147} DEN-modified electrode was held at −0.25 V in a N_2-purged, 0.10 M $HClO_4$ solution containing 5.0 mM $CuSO_4$ for 100 s. Figure 1 shows a typical Cu stripping voltammogram for Pt_{147}@$Cu_{partial}$ DENs in this same Cu deposition solution. The oxidation peak for UPD Cu on the Pt_{147} DENs (100) facet is at −0.14 *vs* Hg/Hg_2SO_4 (0.51 *vs* NHE), which is consistent with our previous result of ~0.55 V *vs* NHE.[39,40] A stripping voltammogram is also shown for exactly the same electrode but for full monolayer coverage of Cu (Pt_{147}@Cu_{full}, Figure 1). Comparison of the integrated areas under these two peaks indicates that the surface coverage of Cu on Pt_{147}@$Cu_{partial}$, relative to that of Pt_{147}@Cu_{full}, is 57 ± 5% (based on five independent experiments). This value is in good agreement with the number of surface Pt atoms on the (100) facets of an ideal 147 atom cuboctahedron: 54%. Accordingly, we are confident that the (100) facets have been fully and selectively decorated with Cu.

Electrocatalytic Activity. We evaluated the electrochemical properties of Pt_{147} and Pt_{147}@$Cu_{partial}$ DENs by recording rotating disk voltammograms (RDVs) in the presence of a saturated aqueous solution of CO. These scans

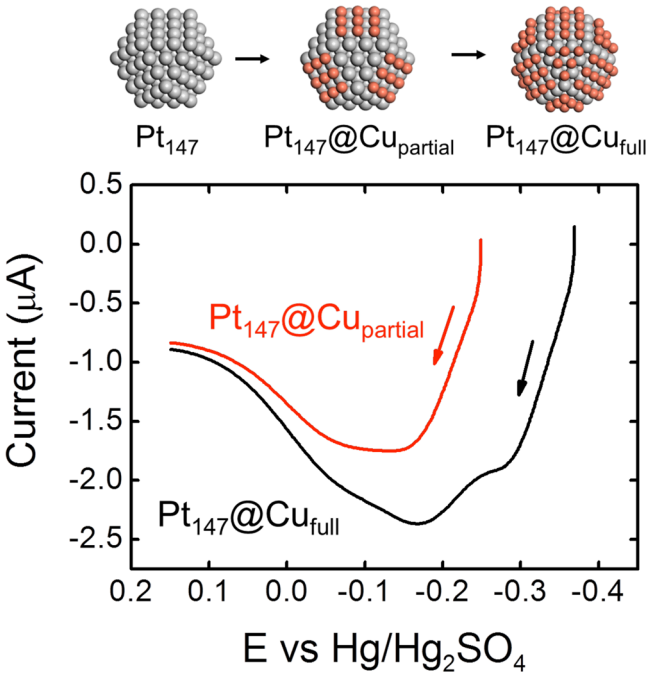

Figure 1. Cu stripping voltammograms recorded using Pt_{147}@$Cu_{partial}$ and Pt_{147}@Cu_{full} DEN-modified GC-RDE in a deaerated 0.10 M $HClO_4$/5.0 mM $CuSO_4$ solution. The voltammograms were obtained by depositing Cu onto Pt_{147} DENs at the appropriate UPD potential for 100 s and then removing it by sweeping the potential from the UPD potential to 0.15 V. Scan rate = 10.0 mV/s.

started at −1.20 V and initially proceeded in the positive direction. Figure 2a, which is an RDV obtained using Pt_{147} DENs, reveals CO oxidation peaks at approximately −0.4 and −0.6 V. The relative positions of these peaks are a consequence of catalyst inhibition. Specifically, during the forward scan, the Pt surface is initially fully covered by CO. The high coverage of CO_{ads} inhibits adsorption of OH, which is required for rapid CO oxidation *via* the previously discussed L−H mechanism (Scheme 1). Hence, no current is observed before E = −0.8 V. When the potential reaches −0.8 V, however, the current begins to increase because OH effectively competes for Pt sites and accelerates oxidation of CO_{ads}. At potentials positive of −0.4 V, the current decreases again, this time because formation of PtO_x passivates the catalyst surface. When the scan is reversed, the current initially increases due to reduction of PtO_x, which results in formation of the original Pt catalyst. However, at more negative potentials, CO once again adsorbs onto the Pt surface and passivates it.[8,11,28,30,41] The two CO oxidation peaks that result from this passivation/depassivation mechanism are separated by ~200 mV.

An RDV for Pt_{147}@$Cu_{partial}$ is provided in Figure 2b. This RDV is similar to that of Pt_{147}, but there are also two obvious differences. First, the forward peak in the P_{147}@$Cu_{partial}$ RDV is broader than that for Pt_{147} (fwhm = 490 and 210 mV, respectively). Second, the onset potential for CO oxidation (defined here as the potential corresponding to 5% of the maximum current) shifts negative by ~300 mV for Pt_{147}@$Cu_{partial}$ compared to Pt_{147}. These observations suggest the presence of new sites on Pt_{147}@$Cu_{partial}$ that are more active for CO oxidation than the Pt-only sites. In other words, CO oxidation occurs more easily at these special sites than at Pt-only sites. As a result, a significant increase in CO oxidation current is observed for Pt_{147}@$Cu_{partial}$ at potentials less than

DOI: 10.1021/acsnano.6b04448
ACS Nano 2016, 10, 8760−8769

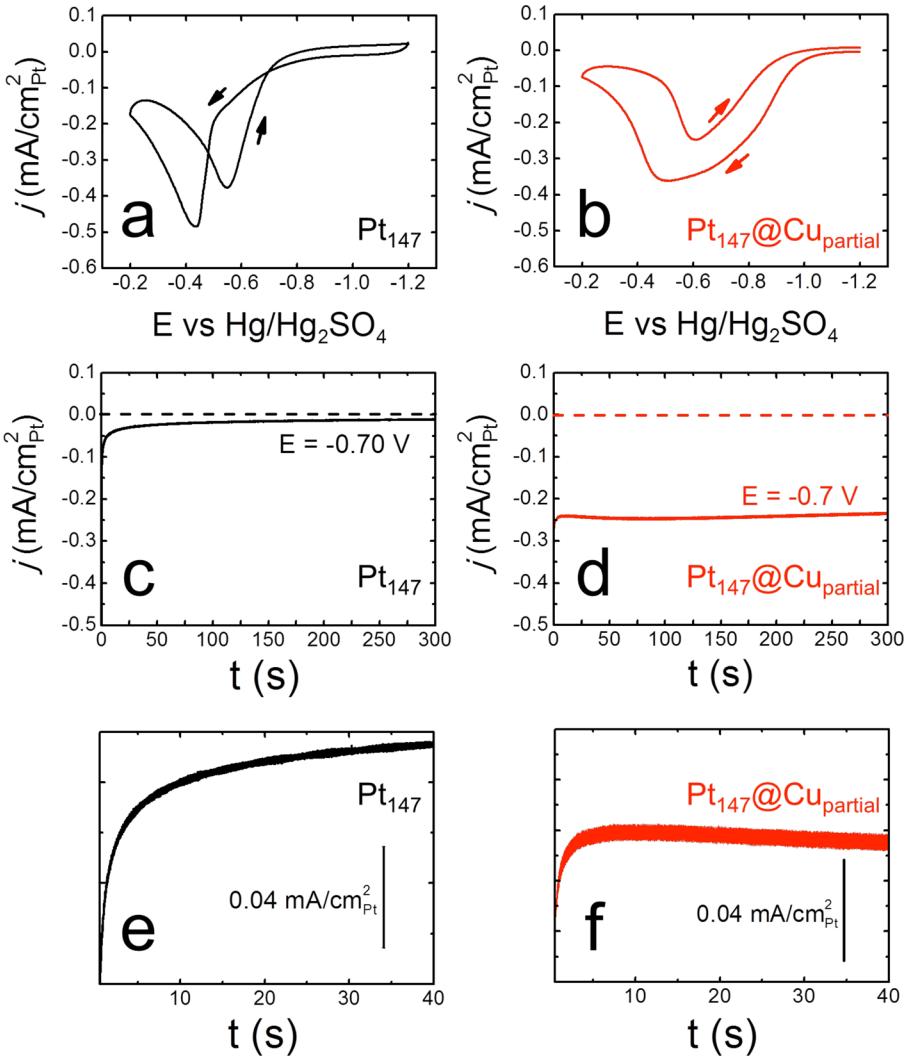

Figure 2. RDVs for CO oxidation at (a) Pt_{147} and (b) $Pt_{147}@Cu_{partial}$ DENs. The scans started at −1.2 V; scan rate = 10.0 mV/s and ω = 1600 rpm. Current *vs* time traces for (c) Pt_{147} and (d) $Pt_{147}@Cu_{partial}$ DENs. The electrode potential was held at −0.70 V. The currents are normalized to the electrochemically active surface area of Pt measured by hydrogen adsorption. (e,f) Expanded views of (c) and (d), respectively, during the first 40 s. The electrode was a GC-RDE, and the solution was CO-saturated 0.10 M NaOH for all experiments.

−0.5 V, resulting in a broader CO oxidation peak and a shift of the onset potential.

Figure 2c,d shows current−time (i−t) traces, obtained at −0.70 V, for CO oxidation at Pt_{147}- and $Pt_{147}@Cu_{partial}$-modified GC-RDEs. At this potential, the steady-state CO oxidation current for $Pt_{147}@Cu$ is ∼0.24 mA/cm^2_{Pt}, which is more than an order of magnitude higher than the value for Pt_{147} DENs of about 0.014 mA/cm^2_{Pt}. This means that the specific activity of $Pt_{147}@Cu_{partial}$ DENs is substantially higher for CO oxidation than Pt_{147} at this potential. In addition to the higher steady-state current, the $Pt_{147}@Cu_{partial}$ catalyst also exhibits slightly better initial stability than Pt_{147}. This is apparent from Figure 2e,f, which shows expanded views of the first parts of the current−time traces of Figure 2c,d, respectively. In Figure 2e, the CO oxidation current for Pt_{147} DENs falls by ∼0.08 mA/cm^2_{Pt} within t = 40 s. In contrast, the current at $Pt_{147}@Cu_{partial}$ DENs (Figure 2f) decreases by less than 0.02 mA/cm^2_{Pt}. Note that transmission electron microscopy (TEM) images of $Pt_{147}@Cu_{partial}$ DENs (Figure S2) do not reveal a change in size after continuous CO oxidation, and therefore, differences in specific activity are not related to gross geometric parameters.

Adsorption of OH on $Pt_{147}@Cu_{partial}$ DENs. We hypothesize that the new active sites on $Pt_{147}@Cu_{partial}$ DENs involve Cu atoms, and that CO oxidation at these sites proceeds *via* the L−H mechanism (Scheme 1). Specifically, CO_{ads} on Pt atoms reacts with the OH_{ads} on Cu atoms to yield the CO_2 product. Because OH adsorbs to Cu at a more negative potential than Pt, CO oxidation on these Cu−Pt sites is accelerated. In contrast, strong CO adsorption on Pt-only DENs excludes OH and hence reduces the rate of CO oxidation. A similar mechanism has previously been proposed by Chorkendorff and co-workers using a PtCu(111) surface alloy for CO oxidation in acidic media.[33] They showed that adsorption of OH onto the Cu sites of the alloy occurs at ∼0.3 V *vs* RHE, which is ∼0.5 V negative of the adsorption potential on Pt(111). This led to a ∼100 mV positive shift of the CO oxidation peak relative to that observed on Pt(111).

To confirm this L−H mechanism for DENs, we first studied the adsorption of OH onto the Cu shell by obtaining cyclic voltammograms (CVs) using Pt_{147} and $Pt_{147}@Cu_{partial}$ DENs in 0.10 M NaOH (Figure 3a). There are two main differences between these CVs. First, the peaks between −0.9 and −1.4 V

DOI: 10.1021/acsnano.6b04448
ACS Nano 2016, 10, 8760−8769

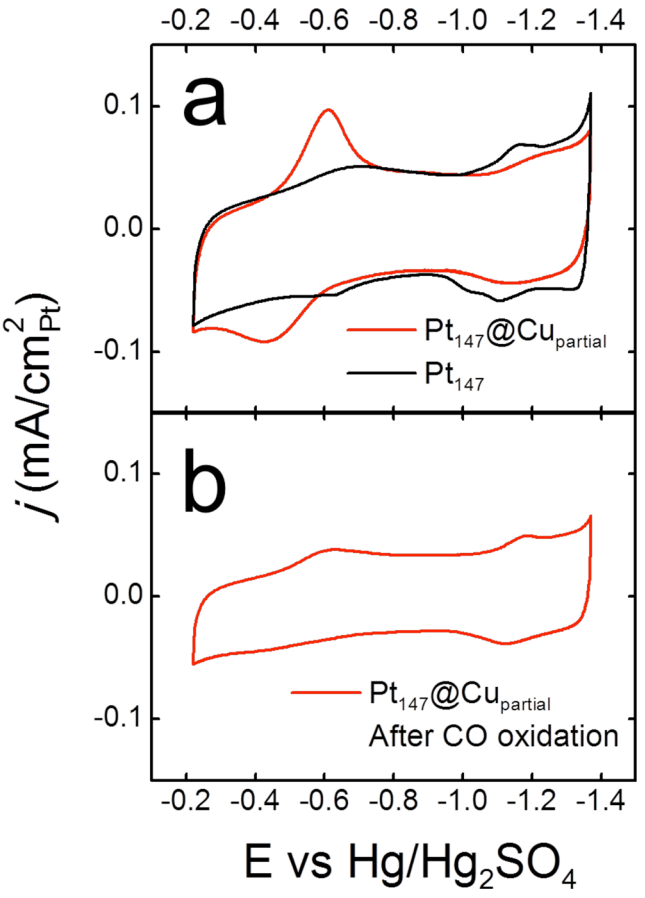

Figure 3. (a) Voltammetric responses of Pt_{147}@$Cu_{partial}$ and Pt_{147} DEN-modified GC-RDEs in deaerated 0.10 M NaOH. Scan rate = 50.0 mV/s. (b) CV obtained using Pt_{147}@$Cu_{partial}$ DENs under the same conditions as in (a), but after oxidation of CO for 5.0 min in CO-saturated 0.10 M NaOH at −0.70 V and ω = 1600 rpm.

associated with hydrogen adsorption and desorption on Pt atoms are suppressed on Pt_{147}@$Cu_{partial}$ relative to Pt_{147} DENs.[39,40,42] This observation is consistent with the presence of a partial coverage of Cu on the Pt_{147}@$Cu_{partial}$ DENs. Second, the Pt_{147}@$Cu_{partial}$ DENs exhibit a pair of peaks at −0.42 and −0.61 V that are absent for the Pt_{147} DENs. These peaks did not change during three consecutive CVs in 0.10 M NaOH (Figure S3). Similar features were observed by Borthen *et al.*[42] when they examined the voltammetry of 2 nm Pt NPs covered with a full monolayer of Cu. Their peaks were at −0.50 and −0.74 V, which are close to those shown in Figure 3a. Using *in situ* X-ray absorption spectroscopy, they were able to assign these two peaks to the transition from Cu^0 to CuO. Adsorption of OH onto Cu, an intermediate step during the Cu^0/CuO transition, starts at the foot of the Cu oxidation peak.[42] Accordingly, these peaks are characteristic of the presence of Cu on the surface of Pt_{147}@$Cu_{partial}$ DENs.

On the basis of the foregoing discussion, it is tempting to suggest a straightforward L−H mechanism for CO oxidation on Pt_{147}@$Cu_{partial}$ DENs. However, there is a problem with this model: adsorption of OH onto the Cu shell of the Pt_{147}@$Cu_{partial}$ DENs starts at about −0.6 V (red trace, Figure 3a). Within the context of the L−H mechanism, this means that CO oxidation should also commence near this potential. In fact, however, CO oxidation begins at the much more negative potential of −1.0 V (Figure 2b). This finding suggests that the simplistic mechanistic view offered in Scheme 1 is not correct, but rather that the DEN structure is driven into a new configuration during CO oxidation. We propose that this new arrangement of atoms binds OH more easily than the Cu shell of the Pt_{147}@$Cu_{partial}$ DENs. In the next two sections, we provide evidence supporting this hypothesis.

Dissolution of the Cu Shell during CO Oxidation. To better identify the true active catalytic sites on Pt_{147}@$Cu_{partial}$, we examined the electrochemistry of Pt_{147}@$Cu_{partial}$ DENs following CO oxidation. Figure 3b shows a CV obtained using Pt_{147}@$Cu_{partial}$ DENs in CO-free 0.1 M NaOH after performing CO oxidation for 5.0 min at −0.70 V (just like the experiment represented in Figure 2d). Surprisingly, the pair of peaks present at −0.42 and −0.61 V in Figure 3a are absent after CO oxidation, and the voltammetry is more similar to that of the Pt_{147} DENs (black trace, Figure 3a). Moreover, the X-ray photoelectron spectroscopy (XPS) results in Figure S4 also show loss of the Cu 2p peak after CO oxidation. Subbaraman *et al.* have also reported electrodissolution of transition metals, including Co, Ni, and Cr, during CO oxidation in alkaline electrolytes.[41] They reported that this was caused by consumption of OH_{ads} species during CO oxidation, leading to dissolution of surface atoms from the metal. The partial Cu shells of the Pt_{147}@$Cu_{partial}$ DENs may be unstable for the same reason. In any event, the loss of the main pair of peaks shown in Figure 3a after CO oxidation further suggests that the partial monolayer of Cu is not responsible for electrocatalytic oxidation of CO.

Active Cu Sites on Pt_{147}^{Cu} DENs. Thus far, we have demonstrated that OH groups bound to adlayers of Cu on Pt DENs are not responsible for electrocatalytic oxidation of CO. We have also shown that the catalytic activity of Pt DENs that were previously coated with adlayers of Cu is higher than that of otherwise identical Pt DENs that were never exposed to Cu. We rationalize these seemingly inconsistent findings by postulating the presence of a very small number (below the limit of detection of CV and XPS) of robust, active Cu sites on the Pt DENs after most Cu dissolves. We denote this new species as Pt_{147}^{Cu} and now set out to prove its existence using both experiments and first-principles theory.

Electrochemical methods can be used to estimate the number of active Cu sites following CO-oxidation-induced dissolution of most of the partial Cu shell. The mechanism supporting this analysis, which has literature precedent,[13,19,43] is that CO_{ads} has low surface mobility in alkaline solution and thus reacts slowly with OH_{ads} unless the two are in close proximity. Note also that the surface mobility of CO_{ads} on <2 nm Pt NPs is known to be even more restricted than on larger Pt particles or planar surfaces.[14,44,45] As a result, CO_{ads} near OH_{ads} is oxidized first, while CO_{ads} that is not in close proximity with OH_{ads} requires a higher potential for conversion to CO_2. On the basis of this mechanism, the Koper group has distinguished four different active sites on Pt surfaces: the three low-index faces and kink sites.[19] Several other groups have reported the presence of two CO_{ads} oxidation peaks when Pt surfaces decorated with Ru are used as catalysts.[15,46−48] Specifically, one voltammetric peak originates from CO_{ads} on and around Ru sites, while a second peak corresponds to oxidation of CO_{ads} on Pt sites distant from Ru sites.[49] By analogy, we believe that, on Pt_{147}^{Cu}, CO_{ads} close to Cu sites (and hence OH_{ads}) will be oxidized at more negative potentials than CO_{ads} that are distant from Cu atoms.[33] Accordingly, oxidation of CO_{ads} on Pt_{147} and

DOI: 10.1021/acsnano.6b04448
ACS Nano 2016, 10, 8760−8769

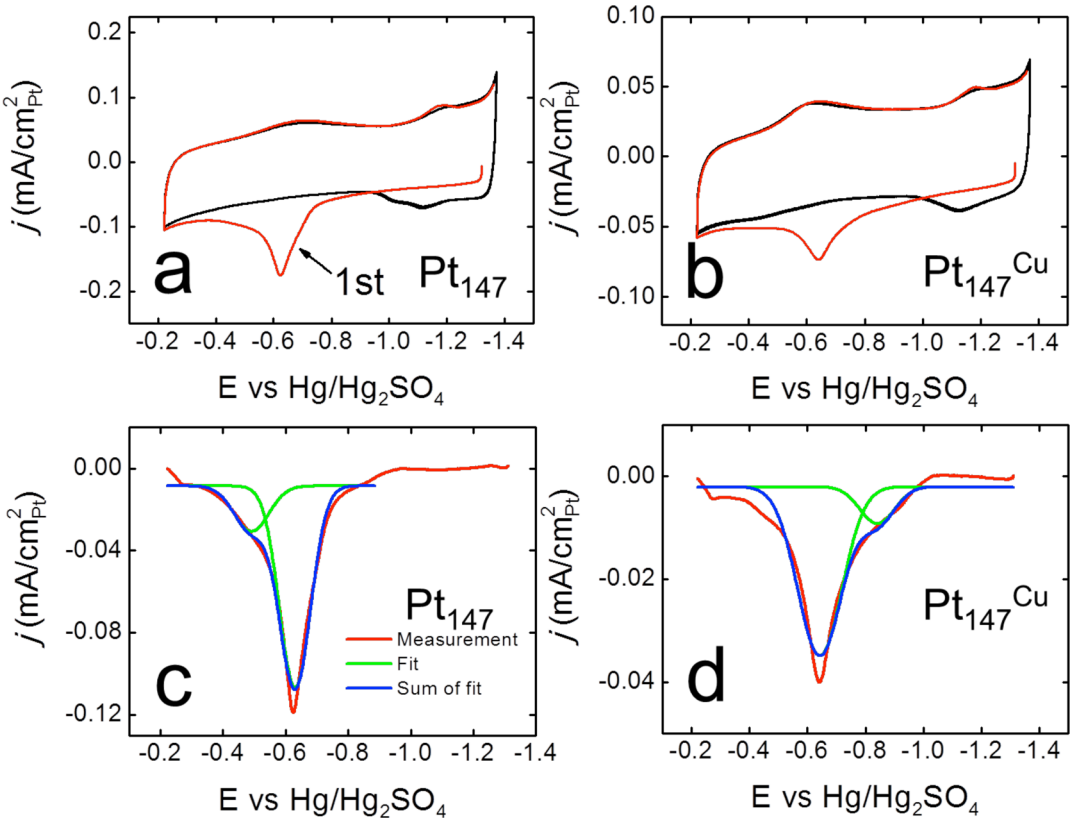

Figure 4. CVs for CO_{ads} on (a) Pt_{147} and (b) Pt_{147}^{Cu} DENs in 0.10 M NaOH. The GC-RDE was prepared by immersing it in a saturated CO solution, setting the electrode potential to −1.32 V for 100 s, and then purging the solution with Ar for 200 s. The scans began at −1.32 V and initially proceeded in the positive direction. Each frame shows three consecutive CVs. The red traces are the first scan, and black ones, which overlay each other, are the final two scans. Scan rate = 50.0 mV/s. The current density is normalized to the electrochemically active surface area of Pt measured by hydrogen adsorption. (c,d) Expanded views of the data in (a) and (b), respectively, with overlaid Gaussian fitting of the CO_{ads} stripping peaks appearing in the first CVs. The peaks are background-subtracted using the second CVs.

Pt_{147}^{Cu} DENs should indirectly, but quantitatively, reveal the presence of Cu sites on the latter.

Figure 4a shows a voltammogram for CO_{ads} on Pt_{147} DENs. This experiment was carried out by immersing the DEN-modified GCE in a 0.10 M NaOH solution, setting the potential at −1.32 V, and then bubbling CO into the solution for 100 s. Next, Ar was introduced into the solution for 200 s to displace dissolved CO. Finally, the potential of the GCE was scanned in the positive direction from −1.32 to −0.20 V and then negative to −1.37 V at 50.0 mV/s three consecutive times. At the beginning of the first scan (red CV), the H desorption peaks associated with Pt atoms are absent because the DEN surface is passivated by CO_{ads}. As the scan continues, however, a peak corresponding to oxidation of CO_{ads} appears at approximately −0.6 V. At this point, the Pt surface is free of CO_{ads}, and so upon scan reversal, the usual peaks for formation of H_{ads} on the Pt surface are present. The second scan (black) reveals peaks for desorption of H_{ads} but not for oxidation of CO_{ads}. The third scan overlays the second, so it is not noticeable. These results are consistent with previous findings.[17,19,29,50]

Figure 4b shows the voltammetry of CO_{ads} obtained using a Pt_{147}^{Cu} DEN-modified GC-RDE. This electrode was prepared starting with a $Pt_{147}@Cu_{parital}$ DEN-modified GC-RDE using the conditions described for Figure 2d, that is, conditions that lead to removal of most of the surface Cu. The CO_{ads} oxidation peak for Pt_{147}^{Cu} DENs is at −0.64 V, which is very close to that for Pt_{147}: −0.63 V. This result suggests that the majority of CO_{ads} on Pt_{147} and Pt_{147}^{Cu} DENs are in a similar chemical environment. This observation is consistent with our previous finding that the Cu partial shell on $Pt_{147}@Cu_{partial}$ DENs is removed after performing bulk CO oxidation.

In addition to the similarity between the positions of the CO_{ads} oxidation peaks on Pt_{147} and Pt_{147}^{Cu} DENs, there are also two noticeable differences. The first difference is that, compared to the Pt_{147}-modified electrode, the CO_{ads} stripping voltammogram obtained using the Pt_{147}^{Cu}-modified electrode exhibits a broad prewave between −0.8 and −1.0 V. This is apparent from a comparison of Figure 4c,d, which shows expanded and deconvoluted views of this potential region. The type of prewave shown in Figure 4d is usually associated with the oxidation of CO_{ads} on Pt terrace sites close to step sites, which act as centers for the nucleation of oxygenated species.[17,19,43,51] Here, however, we believe the prewave, which is absent on the Pt_{147} DENs (Figure 4c), arises from oxygenated species (*i.e.*, OH) present on Cu atoms. It is important to point out that the prewave for the Pt_{147}^{Cu} DENs extends negative to about −1.0 V, which is also the onset potential for bulk CO oxidation (Figure 2b). The second difference between the CVs in Figure 4c,d relates to the prominent postwave, situated between −0.3 and −0.5 V, that is observed just for the Pt_{147} DENs. The absence of this peak in Figure 4d suggests that the least active sites on Pt_{147} DENs are improved following Cu activation.

Up to this point, we have discussed the qualitative features of Figure 4c,d, but we can obtain quantitative information from

DOI: 10.1021/acsnano.6b04448
ACS Nano 2016, 10, 8760−8769

them, as well. Turning first to the Pt_{147} DENs, the major peak at −0.63 V contains ∼80% of the total charge associated with CO_{ads}. The remaining charge is in the postwave at −0.49 V, and it corresponds to oxidation of CO_{ads} at the least active Pt sites. Previous studies using single-crystal Pt electrodes have shown that the least active sites for electrochemical oxidation of CO_{ads} on Pt in alkaline solution are the terraces.[19,43] Step sites are usually more active than the terraces. By analogy, it is reasonable to believe that the least active sites on the Pt_{147} DENs are the facets (analogous to terraces on single crystals). Additional evidence for this conclusion comes from the finding that the relative charge in the postwave, ∼20%, corresponds roughly with the fraction of Pt atoms on facet sites (*i.e.*, those atoms not on edges or corners) of Pt_{147} DENs: 35% (Scheme 2). Therefore, we propose that the major peak at −0.63 V corresponds to CO_{ads} oxidation at the edge and corner sites of Pt_{147} DENs, and that the minor peak at −0.49 V represents CO_{ads} oxidation on the terraces of Pt_{147} DENs.

Scheme 2

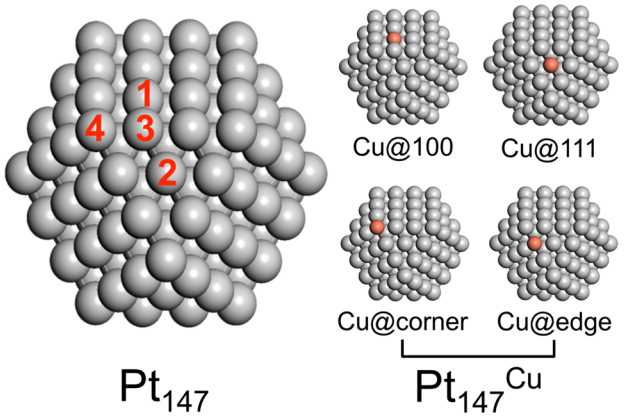

We now consider the interpretation of the voltammetry of Pt_{147}^{Cu} DENs shown in Figure 4d. Here, the major peak contains 85% of the charge associated with CO_{ads}, and the minor peak contains 15%. The major peak at −0.64 V is very close to that for Pt_{147} DENs. As a result, we assign it to oxidation of CO_{ads} at Pt edge and corner sites. The minor peak is a prewave at −0.84 V. Recalling that OH easily adsorbs onto Cu atoms and that OH_{ads} accelerates oxidation of CO_{ads}, we associate this peak with oxidation of CO_{ads} at Pt atoms residing near Cu atoms; that is, sites that promote the L−H mechanism shown in Scheme 1. Assuming OH_{ads} on Cu sites only reacts with its first nearest-neighbor CO_{ads} on Pt, each Cu atom would be responsible for n = 6 to 8 CO_{ads}, depending on the surface atomic packing (hexagonal and square packing, respectively). Accordingly, the percentage of active Cu surface sites should be 15%/n, which is ∼2%. This means that in the case of ∼2 nm diameter Pt_{147}^{Cu} DENs, there will be ∼2 Cu atoms per DEN or <1 Cu site per facet assuming cuboctahedral nanoparticle geometry. Direct detection of this very small number Cu atoms is well below the detection limit of any analytical method that we are aware of, even though they are unambiguously responsible for the observed increase in electrocatalytic activity of Pt_{147}^{Cu} DENs.

Location of Cu on Pt_{147}^{Cu}. It is interesting that the minor CO_{ads} oxidation peaks for Pt_{147} and Pt_{147}^{Cu} DENs have similar sizes (20 and 15%) but are separated by 300 mV (Figure 4c,d). As discussed in the previous section, the minor voltammetric peak for Pt_{147} corresponds to CO_{ads} oxidation on the facets of Pt_{147} DENs, while the minor peak for Pt_{147}^{Cu} is due to CO_{ads} oxidation at Pt atoms close to Cu sites. Taken together, we speculate that the active Cu sites on Pt_{147}^{Cu} are likely located on the facets of Pt DENs instead of at the edges or corners.

To further confirm the location of Cu on Pt_{147}^{Cu}, we used DFT calculations to evaluate several candidate sites (the computational details are given in the Methods section). Each of these models (Scheme 2) consists of an individual Cu surface atom surrounded by Pt, but each Cu atom resides in a unique site on the NP surface. For example, Cu@100 denotes the model having a Cu atom on the (100) facet of Pt_{147}^{Cu}. The calculated binding energies of CO and OH (Eb_{CO} and Eb_{OH}) at each Cu site are provided in Table 1. As a reference, Eb_{CO} and Eb_{OH} are also provided for the Pt_{147} and Pt_{147}@$Cu_{partial}$ NPs. The calculation results indicate that, compared to the equivalent Pt sites, CO binding is much weaker at every Cu site. In contrast, OH binding on the Cu sites is enhanced by ∼100−200 mV compared to most of the Pt sites (the one exception is the Pt corner site). These trends in binding energies allow CO oxidation to proceed through the proposed L−H mechanism, where oxidation of CO_{ads} is driven mainly by OH_{ads} on Cu and CO_{ads} on neighboring Pt atoms. As a consequence, the onset potential for CO oxidation should be shifted roughly by the difference of OH binding on the surface (∼120 to 200 mV), in qualitative agreement with the experimentally measured onset potential difference of ∼300 mV.

Although all candidate models for Pt_{147}^{Cu} are predicted to exhibit CO oxidation activities higher than those for Pt_{147}, their other properties must also be consistent with experimental observations. For example, the active Cu sites of Pt_{147}^{Cu} must bind OH more strongly than Cu present in the partial shell of the Pt_{147}@$Cu_{partial}$ DENs. The formation of OH_{ads} on Pt_{147}^{Cu} commences at potentials as negative as −1.0 V, which is also

Table 1. Calculated CO, OH, and Cu Binding Energies (Eb_{CO}, Eb_{OH}, and Eb_{Cu}, respectively) for the Structural Models Shown in Scheme 2

Pt_{147}^{Cu}				Pt_{147}					
Cu site	Eb_{Cu}	Eb_{CO}(eV)	Eb_{OH}(eV)		Pt site	Eb_{CO}(eV)		Pt site	Eb_{OH}(eV)
Cu@100	−0.36	−0.9	−0.32	1	100	−2.01	1−3	100-br	−0.17
Cu@111	−0.89	−0.44	0.3	2	111	−1.52	332	111-fcc	0.5
Cu@edge	−0.02	−0.94	−0.37	3	edge	−2.06	3−3	edge	−0.25
Cu@corner	−0.23	−1.2	−0.12	4	corner	−2.23	4	corner	−0.51

Pt_{147}@$Cu_{partial}$			
Cu site	Eb_{Cu}	Eb_{CO}(eV)	Eb_{OH}(eV)
Pt_{147}@$Cu_{partial}$	−0.27	−1.73	−0.23

DOI: 10.1021/acsnano.6b04448
ACS Nano 2016, 10, 8760−8769

the onset of CO oxidation (Figure 2b). In contrast, OH_{ads} forms on the partial Cu shell of $Pt_{147}@Cu_{partial}$ at −0.6 V (Figure 3a). Comparison of Eb_{OH} for the candidate models for Pt_{147}^{Cu} and $Pt_{147}@Cu_{partial}$ DENs (Table 1) indicates that OH binds more strongly to the Cu@100 and Cu@edge structures shown in Scheme 2 than to Cu on the $Pt_{147}@Cu_{partial}$ DENs. Therefore, the structures represented in Scheme 2 as Cu@111 and Cu@corner are unlikely to be the active Cu sites on Pt_{147}^{Cu}. In addition, the active Cu sites on Pt_{147}^{Cu} should be more stable than the original partial shell of Cu in $Pt_{147}@Cu_{partial}$ DENs during bulk CO oxidation. Here, we used the Cu binding energy (Eb_{Cu}, Table 1) to theoretically evaluate the stability of Cu in the structures in Scheme 2. According to the calculation results, only Cu@111 and Cu@100 sites are more stable than the Cu partial shell of $Pt_{147}@Cu_{partial}$. Combining these features with the fact that Cu was also initially UPD deposited on the (100) facets of the Pt_{147} DENs, the calculation results suggest that Cu@100 is the most likely structure for Pt_{147}^{Cu}. One last point is worth mentioning. Subsurface Cu atoms are the most robust against leaching,[33] but DFT results indicate that such a structure does not exhibit significant change in Eb_{OH} and Eb_{CO} compared to Pt_{147} (Figure S6). Therefore, they are unlikely to be responsible for the catalytic effects reported here.

SUMMARY AND CONCLUSIONS

In conclusion, we have shown that Pt_{147} DENs decorated with Cu atoms exhibit higher CO oxidation activity than Cu-free Pt_{147} DENs. Experimental results suggest that the improved activity is not directly attributable to the Cu shell present on the $Pt_{147}@Cu_{partial}$ DENs but rather from a small population of active Cu sites on the Pt_{147}^{Cu} DENs (estimated to be <1 site per facet). These isolated Cu atoms provide binding sites for OH on the DEN surface, which provide a basis for rapid CO oxidation *via* the L−H mechanism. Several possible structural models were evaluated using both theory and experiment, and the results indicate that the most likely locations of these Cu sites are on the (100) facets of the Pt_{147}^{Cu} DENs. This finding is significant because it shows how a trace amount of a cocatalytic metal results in a dramatic improvement in catalytic performance.

One final point: direct detection of single, high atomic weight heteroatoms on extended two-dimensional surfaces is challenging.[52−54] The difficulty level is exacerbated when individual light atoms are confined to the surface of <2 nm particles. Indeed, we are unaware of examples in which such materials have been unambiguously chemically analyzed at the single-atom level. Nevertheless, we are attempting to determine the local structure of the special Cu sites described here using EXAFS and ultra-high-resolution TEM. If successful, the outcome of these experiments will be reported in due course.

METHODS

Chemicals. G6-OH dendrimers in methanol were purchased from Dendritech, Inc. (Midland, MI). The methanol was removed under vacuum, and deionized (DI) water was added to yield a solution concentration of 200.0 μM. The following chemicals were used as received without further purification: K_2PtCl_6 and $NaBH_4$ (Aldrich), $CuSO_4$ and NaOH (Fisher Scientific), and $HClO_4$ (70%, ULTREX II ultrapure reagent, J.T. Baker). Ultra-high-purity CO and Ar gas were purchased from Praxair. Solutions were prepared using DI water from a Millipore Milli-Q water system (18.2 MΩ·cm).

Synthesis of Pt_{147} DENs. Pt_{147} DENs were prepared following a previously reported method.[38] Specifically, 147 equiv of K_2PtCl_4 was added to a 10 μM aqueous solution of G6-OH and allowed to react for 3 days. This results in formation of a G6-OH$(Pt^{2+})_{147}$ precursor, in which the stoichiometry reflects the Pt^{2+}:G6-OH solution ratio and is not intended to suggest that every dendrimer incorporates exactly 147 Pt^{2+} ions. A 10-fold excess of 1.0 M $NaBH_4$, dissolved in 0.3 M NaOH, was added to the G6-OH$(Pt^{2+})_{147}$ precursor solution, and then the reaction vessel was tightly sealed. After reacting for overnight, Vulcan EC-72R carbon (1.0 mg per 1.0 mL) was added to the G6-OH(Pt_{147}) DEN solution, and the mixture was sonicated for 5 min to yield an ink composed of Pt_{147} DENs adsorbed to Vulcan carbon.

Electrochemistry. Electrochemical measurements were carried out using a CH Instruments model 1202B potentiostat (Austin, TX). A Hg/Hg_2SO_4 reference electrode and a Pt wire counter electrode (both from CH Instruments) were used for all experiments. The working electrode was a 3.0 mm diameter GC-RDE purchased from Metrohm USA. The GC-RDE was prepared for electrochemical experiments by successive polishing with 1.0, 0.3, and 0.05 μm alumina powder (Buehler) and then sonicating for 5 min to remove the polishing materials from the electrode surface. Finally, a 5.0 μL aliquot of freshly prepared Pt_{147} DEN ink was pipetted onto the GC-RDE, and then it was blown dry under flowing N_2.

Preparation of $Pt_{147}@Cu_{partial}$ and $Pt_{147}@Cu_{full}$ DENs. Cu was deposited onto Pt_{147} DENs following a previously reported procedure with slight modifications.[39,40] First, the surface of the Pt_{147} DENs was cleaned by cycling the working electrode potential 20 times between +0.50 and −0.70 V *vs* Hg/Hg_2SO_4 in 0.10 M N_2-purged $HClO_4$. Second, 100 μL of 0.50 M $CuSO_4$ was added to the 10.0 mL $HClO_4$ cleaning solution. This step was carried out with the GC-RDE immersed in the cleaning solution and at the open-circuit potential (OCP). The electrode potential was then stepped from the OCP to the Cu UPD potential (−0.25 V to prepare $Pt_{147}@Cu_{partial}$ DENs and −0.37 V to prepare $Pt_{147}@Cu_{full}$ DENs) and held there for 100 s. Stripping voltammograms, like those shown in Figure 1, were obtained by sweeping the potential positive from the UPD potential to 0.15 V at 10.0 mV/s.

Bulk CO Oxidation. CO was bubbled into a 0.10 M NaOH solution for 5 min before each bulk CO electro-oxidation experiment. The DEN-modified GC-RDE was then immersed in the CO-saturated NaOH solution. The electrode rotation speed was set to 1600 rpm. The current−time traces were obtained by holding the potential of DEN-modified GC-RDE at −0.7 V. In contrast, the rotating disk voltammograms were obtained by sweeping the potential of GC-RDE from −1.2 to −0.2 V and then back to −1.2 V at 10.0 mV/s.

CO Stripping Voltammetry. The electrochemistry of CO adsorbed to DENs was evaluated using the following procedure. A DEN-modified electrode was immersed in a 0.10 M NaOH solution, its potential was set to −1.32 V, and then CO was bubbled into the solution for 100 s. Ar was then introduced to the solution for 200 s to displace dissolved CO. Finally, the potential was scanned positive to −0.20 V and then negative to −1.37 V at 50.0 mV/s for three cycles.

TEM Analysis. TEM micrographs of Pt_{147} and $Pt_{147}@Cu_{partial}$ DENs were obtained using a JEOL 2010F TEM. The Pt_{147} samples were prepared by dropping ∼1 μL of freshly prepared DEN ink onto carbon-coated copper TEM grids (400 mesh, Electron Microscopy Sciences) and then drying in a stream of N_2 for <1 min. The $Pt_{147}@Cu_{partial}$ samples were prepared by being wiped by a TEM grid across the surface of a GC-RDE modified with $Pt_{147}@Cu_{partial}$ DENs (immobilized on Vulcan carbon) and being dried under N_2 flow after all electrochemical measurements were complete. Gatan Digital Micrograph was used to determine the size distribution of the DENs.

XPS Analysis. XPS data were collected using a Kratos Axis Ultra spectrometer having a monochromatic Al KR X-ray source. The Pt_{147} DEN sample was prepared by dropcasting 10.0 μL of the DEN ink onto a ∼1 cm × ∼1 cm glassy carbon chip. The $Pt_{147}@Cu_{full}$ sample was prepared by carrying out Cu UPD on Pt_{147} DENs (confined to a glassy carbon chip) using a home-built Teflon electrochemical cell. Note that in this experiment we used $Pt_{147}@Cu_{full}$, which has a full monolayer of Cu, in order to improve the signal-to-noise ratio of the XPS spectra. This change does not affect our interpretations of the results because the $Pt_{147}@Cu_{full}$ DENs show an activity toward CO

DOI: 10.1021/acsnano.6b04448
ACS Nano 2016, 10, 8760−8769

oxidation very similar to that of the $Pt_{147}@Cu_{partial}$ DENs, as shown in Figure S5.

Computational Methods. All binding energies were calculated using spin-polarized DFT and the Vienna ab initio simulation package.[55,56] Core electrons were described using the projector-augmented wave method.[57,58] Kohn–Sham single-electron wave functions were expanded in a plane-wave basis with a kinetic energy cutoff of 280 eV to describe the valence electrons. The generalized gradient approximation, using the Perdew–Wang 91 functional, was chosen to evaluate the exchange-correlation energy.[59] All atoms in the nanoparticle were allowed to relax; geometries were considered optimized when the force on each atom was <0.005 eV/Å. Convergence was checked by increasing the energy cutoff to 400 eV, and the CO binding energy on a nanoparticle was found to change by only 1 meV (<0.1%).

CO and OH binding energies, Eb_{CO} and Eb_{OH}, respectively, were calculated using the following equation:

$$Eb(A) = E(A^*) - E(^*) - E(A)$$

where $E(A^*)$ is the total energy of nanoparticles with adsorbates A (A = CO or OH) calculated by DFT, $E(^*)$ is the total energy of clean nanoparticles calculated by DFT, and $E(A)$ is the reference energy for A. The energies of CO and $H_2O-1/2H_2$ in the gas phase were used as $E(CO)$ and $E(OH)$, respectively. Eb_{Cu} is defined as the energy required to remove isolated Cu atoms from the corresponding Pt_{147}^{Cu} (Scheme 2) nanoparticles and is referenced to Cu bulk. Although this binding energy does not account for the exact thermodynamics of the leaching process, it allows us to estimate the relative stability of single Cu atoms at present on different sites as well as the corresponding shift of the Cu dissolution potential.[60]

ASSOCIATED CONTENT

Supporting Information

The Supporting Information is available free of charge on the ACS Publications website at DOI: 10.1021/acsnano.6b04448.

TEM images and particle size distributions, CVs of the $Pt_{147}@Cu_{partial}$ DENs in deaerated 0.1 M NaOH, XPS results, current–time traces for CO oxidation on $Pt_{147}@Cu_{full}$ DENs, and calculations for subsurface Cu atoms (PDF)

AUTHOR INFORMATION

Corresponding Authors

*E-mail: henkelman@utexas.edu.

*E-mail: crooks@cm.utexas.edu.

Notes

The authors declare no competing financial interest.

ACKNOWLEDGMENTS

We gratefully acknowledge support from the National Science Foundation under the DMREF program, Grant No. 1534177. We also thank the Robert A. Welch Foundation (Grants F-0032 and F-1841) for sustained support of our research. This work was also supported by the National Research Foundation of Korea funded by the Ministry of Science, ICT and Future Planning (NRF-2014S1A2A2028540).

REFERENCES

(1) Ianniello, R.; Schmidt, V. M.; Stimming, U.; Stumper, J.; Wallau, A. CO Adsorption and Oxidation on Pt and PtRu Alloys: Dependence on Substrate Composition. *Electrochim. Acta* **1994**, *39*, 1863–1869.

(2) Gasteiger, H. A.; Markovic, N.; Ross, P. N.; Cairns, E. J. Carbon Monoxide Electrooxidation on Well-Characterized Platinum-Ruthenium Alloys. *J. Phys. Chem.* **1994**, *98*, 617–625.

(3) Marković, N. M.; Gasteiger, H. A.; Ross, P. N., Jr; Jiang, X.; Villegas, I.; Weaver, M. J. Electro-Oxidation Mechanisms of Methanol and Formic Acid on Pt-Ru Alloy Surfaces. *Electrochim. Acta* **1995**, *40*, 91–98.

(4) Gasteiger, H. A.; Markovic, N. M.; Ross, P. N. H_2 and CO Electrooxidation on Well-Characterized Pt, Ru, and Pt-Ru. 1. Rotating Disk Electrode Studies of the Pure Gases Including Temperature Effects. *J. Phys. Chem.* **1995**, *99*, 8290–8301.

(5) Schmidt, T. J.; Noeske, M.; Gasteiger, H. A.; Behm, R. J.; Britz, P.; Brijoux, W.; Bönnemann, H. Electrocatalytic Activity of PtRu Alloy Colloids for CO and CO/H_2 Electrooxidation: Stripping Voltammetry and Rotating Disk Measurements. *Langmuir* **1997**, *13*, 2591–2595.

(6) Massong, H.; Tillmann, S.; Langkau, T.; Abd El Meguid, E. A.; Baltruschat, H. On the Influence of Tin and Bismuth UPD on Pt(111) and Pt(332) on the Oxidation of CO. *Electrochim. Acta* **1998**, *44*, 1379–1388.

(7) Koper, M. T. M.; Jansen, A. P. J.; van Santen, R. A.; Lukkien, J. J.; Hilbers, P. A. J. Monte Carlo Simulations of a Simple Model for the Electrocatalytic CO Oxidation on Platinum. *J. Chem. Phys.* **1998**, *109*, 6051–6062.

(8) Marković, N. M.; Schmidt, T. J.; Grgur, B. N.; Gasteiger, H. A.; Behm, R. J.; Ross, P. N. Effect of Temperature on Surface Processes at the Pt(111)–Liquid Interface: Hydrogen Adsorption, Oxide Formation, and CO Oxidation. *J. Phys. Chem. B* **1999**, *103*, 8568–8577.

(9) Lin, W. F.; Zei, M. S.; Eiswirth, M.; Ertl, G.; Iwasita, T.; Vielstich, W. Electrocatalytic Activity of Ru-Modified Pt(111) Electrodes toward CO Oxidation. *J. Phys. Chem. B* **1999**, *103*, 6968–6977.

(10) Schmidt, T. J.; Grgur, B. N.; Behm, R. J.; Markovic, N. M.; Ross, P. N., Jr. Bi Adsorption on Pt(111) in Perchloric Acid Solution: A Rotating Ring-Disk Electrode and XPS Study. *Phys. Chem. Chem. Phys.* **2000**, *2*, 4379–4386.

(11) Schmidt, T. J.; Ross, P. N.; Markovic, N. M. Temperature-Dependent Surface Electrochemistry on Pt Single Crystals in Alkaline Electrolyte: Part 1: CO Oxidation. *J. Phys. Chem. B* **2001**, *105*, 12082–12086.

(12) Brankovic, S. R.; Wang, J. X.; Adžić, R. R. Pt Submonolayers on Ru Nanoparticles: A Novel Low Pt Loading, High CO Tolerance Fuel Cell Electrocatalyst. *Electrochem. Solid-State Lett.* **2001**, *4*, A217–A220.

(13) Zhdanov, V. P.; Kasemo, B. Simulation of CO Electrooxidation on nm-Sized Supported Pt Particles: Stripping Voltammetry. *Chem. Phys. Lett.* **2003**, *376*, 220–225.

(14) Maillard, F.; Eikerling, M.; Cherstiouk, O. V.; Schreier, S.; Savinova, E.; Stimming, U. Size Effects on Reactivity of Pt Nanoparticles in CO Monolayer Oxidation: The Role of Surface Mobility. *Faraday Discuss.* **2004**, *125*, 357–377.

(15) Spendelow, J. S.; Babu, P. K.; Wieckowski, A. Electrocatalytic Oxidation of Carbon Monoxide and Methanol on Platinum Surfaces Decorated with Ruthenium. *Curr. Opin. Solid State Mater. Sci.* **2005**, *9*, 37–48.

(16) Wei, Z. D.; Li, L. L.; Luo, Y. H.; Yan, C.; Sun, C. X.; Yin, G. Z.; Shen, P. K. Electrooxidation of Methanol on UPD-Ru and UPD-Sn Modified Pt Electrodes. *J. Phys. Chem. B* **2006**, *110*, 26055–26061.

(17) Spendelow, J. S.; Goodpaster, J. D.; Kenis, P. J. A.; Wieckowski, A. Mechanism of CO Oxidation on Pt(111) in Alkaline Media. *J. Phys. Chem. B* **2006**, *110*, 9545–9555.

(18) Falsig, H.; Hvolbæk, B.; Kristensen, I. S.; Jiang, T.; Bligaard, T.; Christensen, C. H.; Nørskov, J. K. Trends in the Catalytic CO Oxidation Activity of Nanoparticles. *Angew. Chem.* **2008**, *120*, 4913–4917.

(19) Garcia, G.; Koper, M. T. M. Stripping Voltammetry of Carbon Monoxide Oxidation on Stepped Platinum Single-Crystal Electrodes in Alkaline Solution. *Phys. Chem. Chem. Phys.* **2008**, *10*, 3802–3811.

(20) Falsig, H.; Hvolbæk, B.; Kristensen, I. S.; Jiang, T.; Bligaard, T.; Christensen, C. H.; Nørskov, J. K. Trends in the Catalytic CO Oxidation Activity of Nanoparticles. *Angew. Chem., Int. Ed.* **2008**, *47*, 4835–4839.

(21) Lee, S. W.; Chen, S.; Sheng, W.; Yabuuchi, N.; Kim, Y.-T.; Mitani, T.; Vescovo, E.; Shao-Horn, Y. Roles of Surface Steps on Pt

DOI: 10.1021/acsnano.6b04448
ACS Nano 2016, 10, 8760–8769

Nanoparticles in Electro-Oxidation of Carbon Monoxide and Methanol. *J. Am. Chem. Soc.* **2009**, *131*, 15669−15677.
(22) Du, Y.; Wang, C. Preparation Ru, Bi Monolayer Modified Pt Nanoparticles as the Anode Catalyst for Methanol Oxidation. *Mater. Chem. Phys.* **2009**, *113*, 927−932.
(23) Rodriguez, P.; Garcia-Araez, N.; Koverga, A.; Frank, S.; Koper, M. T. M. CO Electroxidation on Gold in Alkaline Media: A Combined Electrochemical, Spectroscopic, and DFT Study. *Langmuir* **2010**, *26*, 12425−12432.
(24) Bernechea, M. a.; García-Rodríguez, S.; Terreros, P.; de Jesús, E.; Fierro, J. L. G.; Rojas, S. Synthesis of Core−Shell PtRu Dendrimer-Encapsulated Nanoparticles. Relevance as Electrocatalysts for CO Oxidation†. *J. Phys. Chem. C* **2011**, *115*, 1287−1294.
(25) Ochal, P.; Gomez de la Fuente, J. L.; Tsypkin, M.; Seland, F.; Sunde, S.; Muthuswamy, N.; Rønning, M.; Chen, D.; Garcia, S.; Alayoglu, S.; Eichhorn, B. CO Stripping as an Electrochemical Tool for Characterization of Ru@Pt Core-Shell Catalysts. *J. Electroanal. Chem.* **2011**, *655*, 140−146.
(26) Kim, J.; Kim, S.; Rhee, C. K. Preoxidation of CO on Os-Modified Pt(111): A Comparison with Ru-Modified Pt(111). *Langmuir* **2011**, *27*, 2044−2051.
(27) Li, H.; Li, L.; Pedersen, A.; Gao, Y.; Khetrapal, N.; Jónsson, H.; Zeng, X. C. Magic-Number Gold Nanoclusters with Diameters from 1 to 3.5 nm: Relative Stability and Catalytic Activity for CO Oxidation. *Nano Lett.* **2015**, *15*, 682−688.
(28) Rudnev, A. V.; Kuzume, A.; Fu, Y.; Wandlowski, T. CO Oxidation on Pt(100): New Insights Based on Combined Voltammetric, Microscopic and Spectroscopic Experiments. *Electrochim. Acta* **2014**, *133*, 132−145.
(29) Luo, L.; Zhang, L.; Henkelman, G.; Crooks, R. M. Unusual Activity Trend for CO Oxidation on Pd_xAu_{140-x}@Pt Core@Shell Nanoparticle Electrocatalysts. *J. Phys. Chem. Lett.* **2015**, *6*, 2562−2568.
(30) Kodama, K.; Morimoto, Y.; Strmcnik, D. S.; Markovic, N. M. The Role of Non-Covalent Interactions on CO Bulk Oxidation on Pt Single Crystal Electrodes in Alkaline Electrolytes. *Electrochim. Acta* **2015**, *152*, 38−43.
(31) Gasteiger, H. A.; Markovic, N.; Ross, P. N.; Cairns, E. J. Methanol Electrooxidation on Well-Characterized Platinum-Ruthenium Bulk Alloys. *J. Phys. Chem.* **1993**, *97*, 12020−12029.
(32) Wickman, B.; Seidel, Y. E.; Jusys, Z.; Kasemo, B.; Behm, R. J. Fabrication of Pt/Ru Nanoparticle Pair Arrays with Controlled Separation and Their Electrocatalytic Properties. *ACS Nano* **2011**, *5*, 2547−2558.
(33) Bandarenka, A. S.; Varela, A. S.; Karamad, M.; Calle-Vallejo, F.; Bech, L.; Perez-Alonso, F. J.; Rossmeisl, J.; Stephens, I. E. L.; Chorkendorff, I. Design of an Active Site Towards Optimal Electrocatalysis: Overlayers, Surface Alloys and near-Surface Alloys of Cu/Pt(111). *Angew. Chem., Int. Ed.* **2012**, *51*, 11845−11848.
(34) Herrero, E.; Buller, L. J.; Abruña, H. D. Underpotential Deposition at Single Crystal Surfaces of Au, Pt, Ag and Other Materials. *Chem. Rev.* **2001**, *101*, 1897−1930.
(35) Slanac, D. A.; Hardin, W. G.; Johnston, K. P.; Stevenson, K. J. Atomic Ensemble and Electronic Effects in Ag-Rich AgPd Nanoalloy Catalysts for Oxygen Reduction in Alkaline Media. *J. Am. Chem. Soc.* **2012**, *134*, 9812−9819.
(36) Roger, I.; Symes, M. D. Efficient Electrocatalytic Water Oxidation at Neutral and High pH by Adventitious Nickel at Nanomolar Concentrations. *J. Am. Chem. Soc.* **2015**, *137*, 13980−13988.
(37) Boucher, M. B.; Zugic, B.; Cladaras, G.; Kammert, J.; Marcinkowski, M. D.; Lawton, T. J.; Sykes, E. C. H.; Flytzani-Stephanopoulos, M. Single Atom Alloy Surface Analogs in $Pd_{0.18}Cu_{15}$ Nanoparticles for Selective Hydrogenation Reactions. *Phys. Chem. Chem. Phys.* **2013**, *15*, 12187−12196.
(38) Knecht, M. R.; Weir, M. G.; Myers, V. S.; Pyrz, W. D.; Ye, H.; Petkov, V.; Buttrey, D. J.; Frenkel, A. I.; Crooks, R. M. Synthesis and Characterization of Pt Dendrimer-Encapsulated Nanoparticles: Effect of the Template on Nanoparticle Formation. *Chem. Mater.* **2008**, *20*, 5218−5228.
(39) Carino, E. V.; Crooks, R. M. Characterization of Pt@Cu Core@Shell Dendrimer-Encapsulated Nanoparticles Synthesized by Cu Underpotential Deposition. *Langmuir* **2011**, *27*, 4227−4235.
(40) Carino, E. V.; Kim, H. Y.; Henkelman, G.; Crooks, R. M. Site-Selective Cu Deposition on Pt Dendrimer-Encapsulated Nanoparticles: Correlation of Theory and Experiment. *J. Am. Chem. Soc.* **2012**, *134*, 4153−4162.
(41) Subbaraman, R.; Danilovic, N.; Lopes, P. P.; Tripkovic, D.; Strmcnik, D.; Stamenkovic, V. R.; Markovic, N. M. Origin of Anomalous Activities for Electrocatalysts in Alkaline Electrolytes. *J. Phys. Chem. C* **2012**, *116*, 22231−22237.
(42) Borthen, P.; Hwang, B.-J.; Strehblow, H.-H.; Kolb, D. M. In Situ Observation of the Potential-Dependent Chemical State and Structure of a Cu Monolayer Deposited on the Surface of Carbon-Supported Platinum Clusters. *J. Phys. Chem. B* **2000**, *104*, 5078−5083.
(43) Farias, M. J. S.; Busó-Rogero, C.; Gisbert, R.; Herrero, E.; Feliu, J. M. Influence of the CO Adsorption Environment on Its Reactivity with (111) Terrace Sites in Stepped Pt Electrodes under Alkaline Media. *J. Phys. Chem. C* **2014**, *118*, 1925−1934.
(44) Becerra, L. R.; Klug, C. A.; Slichter, C. P.; Sinfelt, J. H. Nmr Study of Diffusion of Carbon Monoxide on Alumina-Supported Platinum Clusters. *J. Phys. Chem.* **1993**, *97*, 12014−12019.
(45) Tong, Y. Y.; Oldfield, E.; Wieckowski, A. Diffusion on a Nanoparticle Surface as Revealed by Electrochemical NMR. *Faraday Discuss.* **2002**, *121*, 323−330.
(46) Spendelow, J. S.; Lu, G. Q.; Kenis, P. J. A.; Wieckowski, A. Electrooxidation of Adsorbed CO on Pt(1 1 1) and Pt(1 1 1)/Ru in Alkaline Media and Comparison with Results from Acidic Media. *J. Electroanal. Chem.* **2004**, *568*, 215−224.
(47) Waszczuk, P.; Solla-Gullón, J.; Kim, H. S.; Tong, Y. Y.; Montiel, V.; Aldaz, A.; Wieckowski, A. Methanol Electrooxidation on Platinum/Ruthenium Nanoparticle Catalysts. *J. Catal.* **2001**, *203*, 1−6.
(48) Lu, G. Q.; Waszczuk, P.; Wieckowski, A. Oxidation of CO Adsorbed from CO Saturated Solutions on the Pt(111)/Ru Electrode. *J. Electroanal. Chem.* **2002**, *532*, 49−55.
(49) Friedrich, K. A.; Geyzers, K. P.; Linke, U.; Stimming, U.; Stumper, J. CO Adsorption and Oxidation on a Pt(111) Electrode Modified by Ruthenium Deposition: An IR Spectroscopic Study. *J. Electroanal. Chem.* **1996**, *402*, 123−128.
(50) Weir, M. G.; Myers, V. S.; Frenkel, A. I.; Crooks, R. M. In Situ X-Ray Absorption Analysis of ∼ 1.8 nm Dendrimer-Encapsulated Pt Nanoparticles During Electrochemical CO Oxidation. *ChemPhysChem* **2010**, *11*, 2942−2950.
(51) García, G.; Koper, M. T. M. Dual Reactivity of Step-Bound Carbon Monoxide During Oxidation on a Stepped Platinum Electrode in Alkaline Media. *J. Am. Chem. Soc.* **2009**, *131*, 5384−5385.
(52) Yang, X.-F.; Wang, A.; Qiao, B.; Li, J.; Liu, J.; Zhang, T. Single-Atom Catalysts: A New Frontier in Heterogeneous Catalysis. *Acc. Chem. Res.* **2013**, *46*, 1740−1748.
(53) Liang, S.; Hao, C.; Shi, Y. The Power of Single-Atom Catalysis. *ChemCatChem* **2015**, *7*, 2559−2567.
(54) Narula, C. K.; Moses-DeBusk, M. Catalysis on Single Supported Atoms. In *Catalysis by Materials with Well-Defined Structures*; Overbury, S. H., Wu, Z., Eds.; Elsevier: Amsterdam, 2015; Chapter 9, pp 263−274.
(55) Kresse, G. Dissociation and Sticking of H_2 on the Ni(111), (100), and (110) Substrate. *Phys. Rev. B: Condens. Matter Mater. Phys.* **2000**, *62*, 8295−8305.
(56) Kresse, G.; Hafner, J. First-Principles Study of the Adsorption of Atomic H on Ni (111), (100) and (110). *Surf. Sci.* **2000**, *459*, 287−302.
(57) Blöchl, P. Projector Augmented-Wave Method. *Phys. Rev. B: Condens. Matter Mater. Phys.* **1994**, *50*, 17953−17979.
(58) Kresse, G.; Joubert, D. From Ultrasoft Pseudopotentials to the Projector Augmented-Wave Method. *Phys. Rev. B: Condens. Matter Mater. Phys.* **1999**, *59*, 1758−1775.
(59) Hammer, B.; Hansen, L. B.; Nørskov, J. K. Improved Adsorption Energetics within Density-Functional Theory Using

DOI: 10.1021/acsnano.6b04448
ACS Nano 2016, 10, 8760−8769

Revised Perdew-Burke-Ernzerhof Functionals. *Phys. Rev. B: Condens. Matter Mater. Phys.* **1999**, *59*, 7413−7421.
(60) Yancey, D. F.; Zhang, L.; Crooks, R. M.; Henkelman, G. Au@Pt Dendrimer Encapsulated Nanoparticles as Model Electrocatalysts for Comparison of Experiment and Theory. *Chem. Sci.* **2012**, *3*, 1033−1040.

DOI: 10.1021/acsnano.6b04448
ACS Nano 2016, 10, 8760−8769